2226 *Chem. Mater.* **2010,** *22,* 2226–2232
DOI:10.1021/cm9024843

CHEMISTRY OF MATERIALS
Article

Structure−Property Correlation in Iron Oxide Nanoparticle−Clay Hybrid Materials

You-Hwan Son,[†] Jung-Kun Lee,*[,†] Yee Soong,[‡] Donald Martello,[‡] and Minking Chyu[†]

[†]*Department of Mechanical Engineering & Material Science, University of Pittsburgh, Pittsburgh, Pennsylvania 15261, and* [‡]*National Energy Technology Laboratory, U.S. Department of Energy, Pittsburgh, Pennsylvania 15236*

Received August 13, 2009. Revised Manuscript Received February 24, 2010

Heterostructures between montmorillonite and embedded α-Fe_2O_3 nanoparticles are explored to create new hybrid particles with high magnetic response and magnetic-field induced tunability. α-Fe_2O_3 nanoparticles are hybridized to montmorillonite clays by using an intercalation technique. Also, stable aqueous fluids consisting of the heterostructured particles are prepared and the rheology of the fluids under external magnetic field is examined. When α-Fe_2O_3 nanoparticles are embedded in the interlayer space of montmorillonite clays, the magnetization per Fe atom increases at most 60 times. This unique combination of the magnetization and the coercivity is traced to the suppressed growth of embedded α-Fe_2O_3 nanoparticles by the aluminosilicate layers, leading to the size control, anisotropic magnetic interaction, and uniaxial stress of two-dimensionally distributed α-Fe_2O_3 nanoparticles. Furthermore, high magnetization of heterostructured particles leads to strong dependence of fluids' viscosity on the external magnetic field. The present study indicates that the new heterostructured particles have unique magnetic field-dependent properties that are not attainable in individual clay or iron oxide particles.

Introduction

Magnetic nanoparticles dispersed in fluids offer special opportunities to both science and technology for their unique applications in ferrofluids, drug carriers, and cell separation/purification.[1−6] Such remarkable functionalities of the magnetic nanoparticles stem directly from their nanometric size. Low dimensions of the magnetic nanoparticles decreases magnetic anisotropy energy to be comparable to thermal energy at room temperature, which helps the random motion of the magnetic nanoparticles.[7−9] Consequently, the magnetic nanoparticles show their unique dependence on magnetic field, called superparamagnetism, which allows for a reversible transition between a pseudoparamagnetic state and a pseudoferromagnetic state by applying the external magnetic field.[10,11]

To harness the superparamagnetism of the magnetic nanoparticles, it is important to control the dispersion and agglomeration of the nanoparticles in liquid media. When strong magnetic field is applied, the magnetic nanoparticles can make big agglomerates which are stable even after the magnetic field is removed. An increase in an apparent particle size by the agglomeration, in turn, suppresses superparamagnetism, produces permanent magnetization, and prevents fully reversible response of the magnetic dipoles to the external magnetic field. To prevent the agglomeration of magnetic nanoparticles, it is requested to keep a certain distance between the magnetic nanoparticles. Recently, great efforts have been placed on research to prepare hybrid materials to fully utilize the superparamagnetism by hybridizing the magnetic nanoparticles with hydrophilic spacers such as a block copolymer coating and a silica shell.[12,13] However, these surface modification techniques have chances to decrease magnetic response and surface area of the hybrid materials. This is harmful in

*Corresponding author. E-mail: jul37@pitt.edu.

(1) Won, J.; Kim, M.; Yi, Y.-W.; Kim, Y. H.; Jung, N.; Kim, T. K. *Science* **2005**, *309*, 121.
(2) Weissleder, R.; Kelly, K.; Sun, E. Y.; Shtatland, T.; Josephson, L. *Nat. Biotechnol.* **2005**, *23*, 1418.
(3) Huh, Y.-M.; Jun, Y.-W.; Song, H.-T.; Kim, S.; Choi, J.-S.; Lee, J.-H.; Yoon, S.; Kim, K.-S.; Shin, J.-S.; Suh, J.-S.; Cheon, J. *J. Am. Chem. Soc.* **2005**, *127*, 12387.
(4) Stavroyiannis, S.; Panagiotopoulos, I.; Niarchos, D.; Christodiulides, J. A.; Zhang, Y.; Hadjipanayis, G. C. *Appl. Phys. Lett.* **1998**, *73*, 3453.
(5) Qin, J.; Asempah, I.; Laurent, S.; Fornara, A.; Muller, R. N.; Muhammed, M. *Adv. Mater.* **2009**, *21*, 1.
(6) Kumar, C. S. S. R.; Hormes, J.; Leuschner, C. In *Nanofabrication towards Biomedical Applications*; Wiley-VCH: Weinheim, Germany, 2005.
(7) Walker, M.; Diebel, C.; Haugh, C.; Pankhurst, P.; Montgomery, J.; Green, C. *Nature* **1997**, *390*, 371.
(8) Jun, Y.-W.; Seo, J.-W.; Cheon, J. *Acc. Chem. Res.* **2008**, *41*, 179.
(9) Hyeon, T. *Chem. Commun.* **2003**, 927.
(10) De Gans, B. J.; Duin, N. J.; Van den Ende, D.; Mellema, J. *J. Chem. Phys.* **2000**, *113*, 2032.
(11) Lopez-Lopez, M. T.; Kuzhir, P.; Lacis, S.; Bossis, G.; Gonźalez-Caballero, F.; Duŕan, J. D. G. *J. Phys.: Condens. Matter* **2006**, *18*, 2803.
(12) (a) Xu, X. L.; Friedman, G.; Humfeld, K. D.; Majetich, S. A.; Asher, S. A. *Adv. Mater.* **2001**, *13*, 1681. (b) Ge, J. P.; Hu, Y. X.; Zhang, T. R.; Yin, Y. D. *J. Am. Chem. Soc.* **2007**, *129*, 894.
(13) (a) Lu, Y.; Yin, Y. D.; Li, Z.; Xia, Y. Y *Nano Lett.* **2002**, *2*, 785. (b) Sudimack, J.; Lee, R. J. *Adv. Drug Delivery Rev.* **2000**, *41*, 147.

Published on Web 03/16/2010

maximizing the saturated magnetization of the hybrid particles per unit volume or subsequently conjugating the hybrid materials with catalytic or biofunctional molecules. Therefore, it is still challenging to find superpargamagnetic hybrid particles with large saturated magnetization and high surface area and to fully utilize the superparamanetism of the magnetic nanoparticles in the fluids for various applications.

Montmorillonite, one of layered aluminosilicate minerals, can provide a superior matrix to hybridize the magnetic nanoparticles because of its unique physicochemical properties such as tunable large interlayer space. The cation exchange capacity of the montmorillonite makes them very suitable for embedding metal oxide nanoparticles via an intercalative route. Several types of metal oxide nanoparticle such as Al_2O_3, ZrO_2, TiO_2, ZnO, $SiO_2-Fe_2O_3$, and SiO_2-TiO_2 and SiO_2-CoO have been successfully introduced to the interlayer space within the anisotropic lamellar structure of montmorillonite.[14−17] In addition, a permanent negative charge on the basal surface of montmorillonite is easily modified and contributes to a hydrophilic property.[18−21]

Among the metal oxide particles, α-Fe_2O_3 has received much attention because of its widespread application as catalyst, pigment, senor, and raw material for synthesizing γ-Fe_2O_3.[22−24] In addition to conventional applications, montmorillonite-α-Fe_2O_3 hybrid particle might also be used for modification and encapsulation of various functional molecules and this is likely to lead to novel applications in areas such as drug delivery and medical diagnosis. In these regards, several research groups have studied on embedding iron oxide particles. However, the previous works have suggested that different phases of iron oxide particles are located on external surface of montmorillonite when iron polycations are prepared at room temperature, regardless of intercalation conditions.[25,26]

Herein, we present a new montmorillonite-α-Fe_2O_3 hybrid material with clean external surfaces through intercalating more highly charged and stable iron polycation into the interlayer space of montmorillonite. We have carried out the systematic characterizations of crystal structure and magnetic properties of resulting new hybrid material using X-ray diffraction (XRD), transmission electron microscope (TEM), Raman spectroscopy, and vibrating sample magnetometer (VSM). Using this new hybrid particle, we prepared aqueous fluids and investigated the response of the particles to the external magnetic field within the fluids.

Experimental Procedure

Material and Chemicals. Na^+-montmorillonite (Kunipia F, Kunimine Corp) was used as a starting clay material with the chemical formula of $Na_{0.35}K_{0.01}Ca_{0.02}(Si_{3.89}Al_{0.11})(Al_{1.60}Mg_{0.32}Fe_{0.08})O_{10}(OH)_2 \cdot nH_2O$ with a cation exchange capacity (CEC) of 100 mequiv/100g. Reagent grade $FeCl_3 \cdot 6H_2O$ (Aldrich, 97%) and NaOH (Mallinckrodt) were used to synthesize polycation precursors.

Synthesis and Characterization. Fe polycations were produced by reacting 0.2 mol of $FeCl_3$ and 0.4 mol of NaOH in deionized water (1 L) at 25 or 70 °C. Then, 0.07 mol of polycations was added to a 100 mL aqueous suspension of 1 wt % montmorillonite particles and exchanged with Na^+ ions of montmorillonite at 25 °C. The iron oxide−clay nanohybrid (ICNH)s were collected by centrifugation, washed thoroughly with deionized water several times, and freeze-dried to remove residual water. A part of the dried particles were annealed at 550 °C in N_2 to convert Fe polycations to iron oxide. The powder XRD measurements of synthesized particles were carried out using Philips PW 1810 diffractometer (Cu Kα radiation, $\lambda = 1.54184$ Å). Low-angle XRD measurement was performed to verify the presence of the montmorillonite (001) peak. In the 2θ range from 2 to 10°, additional Fe filter, 1/32″ slit, and monochromator were attached to prevent incident beam and randomly scattered beam from hitting the detector. The microstructure of particles was analyzed using field emission-scanning electron microscope (FE-SEM, Philips, XL 30) and transmission electron microscope (TEM, Jeol, 200CX). Zeta potentials of Fe polycation were measured with a ZetaPALS (Brookhaven, USA). For an accurate measurement of surface potential, samples were placed in glass cells with Pd electrodes at 25 °C. Attenuated total reflection Fourier transform infrared spectroscopy (ATR-FTIR, Thermo, Nicolet 6700) was used to monitor the sequential change in chemical species. Raman spectrum were measured by Renishaw inVia Raman microscope with 488 nm Ar laser. Magnetic measurements were performed with VSM (LakeShore 7400). Element analyses were carried out using inductivity coupled plasma (ICP) method (Thermo, ICAP 6000). For ICP analysis, the samples were melted with lithium metaborate at 900 °C and cooled to room temperature. The molten product was then dissolved in 30% HNO_3. Assuming that the Al content of the aluminosilicate layer remains unchanged during the hybridization, the ratio of Fe/(other cations) is 21.37% for as-grown ICNH particles of 25 °C aged polycations and 18.20% for as-grown ICNH particles of 70 °C aged polycations. Rheological measurements were performed using a rotational rheometer (Anton Parr, MCR 300) with the magneto-rheological device. When the effect of magnetic field on the rheology of the fluids was measured, the homogeneous magnetic field was set perpendicular to the direction of shear flow.

(14) Salgueiriño-Maceira, V.; Correa-Duarte, M. A. *Adv. Mater.* **2007**, *19*, 4131.
(15) Theil Kuhn, L.; Bojesen, A.; Timmermann, L.; Fauth, K.; Goering, E.; Johnson, E.; Meedom Nielsen, M.; Mørup, S. *J. Magn. Magn. Mater.* **2004**, *272*, 1485.
(16) (a) Choy, J.-H.; Jung, H.; Han, Y. S.; Yoon, J. B.; Shul, Y. G.; Kim, H. J. *Chem. Mater.* **2002**, *14*, 3823. (b) Hur, S. G.; Kim, T. W.; Hwang, S. J.; Hwang, S.-H.; Yang, J. H.; Choy, J.-H. *J. Phys. Chem. B* **2006**, *110*, 1599.
(17) (a) Bornholdt, K.; Corker, J. M.; Evans, J.; Rummey, J. M. *Inorg. Chem.* **1991**, *30*, 2. (b) Drljaca, A.; Anderson, J. R.; Spiccia, L.; Turney, T. W. *Inorg. Chem.* **1992**, *31*, 4894.
(18) Choy, J. -H.; Kwak, S. -Y.; Han, Y. -S.; Kim, B.-W. *Mater. Lett.* **1997**, *33*, 143.
(19) Walcarius, A.; Etienne, M.; Delacote, C. *Anal. Chim. Acta* **2004**, *508*, 87.
(20) Bois, L.; Bonhommé, A.; Ribes, A.; Pais, B.; Raffin, G.; Tessier, F. *Colloids Surf., A* **2003**, *221*, 221.
(21) Bourlinos, A. B.; Chowdhury, D. D.; An, Y. −U.; Zhang., Q.; Archer, L. A.; Giannelis, E. P. *Small* **2005**, *1*, 80.
(22) Faust, B. C.; Hoffmann, M. R.; Bahnemann, D. W. *J. Phys. Chem.* **1989**, *93*, 6371.
(23) Han, J. S.; Bredow, T.; Davey, D. E.; Yu, A. B.; Mulcahy, D. E. *Sens. Actuators, B* **2001**, *75*, 18.
(24) Chen, J.; Xu, L.; Li, W.; Gou, X. *Adv. Mater.* **2005**, *17*, 582.
(25) Yuan, P.; He, H.; Bergaya, F.; Wu, D.; Zhou, Q.; Zhu, J. *Microporous Mesoporous Mater.* **2006**, *88*, 8.
(26) Bourlinos, A. B.; Karakassides, M. A.; Simopoulos, A.; Petridis, D. *Chem. Mater.* **2000**, *12*, 2640.

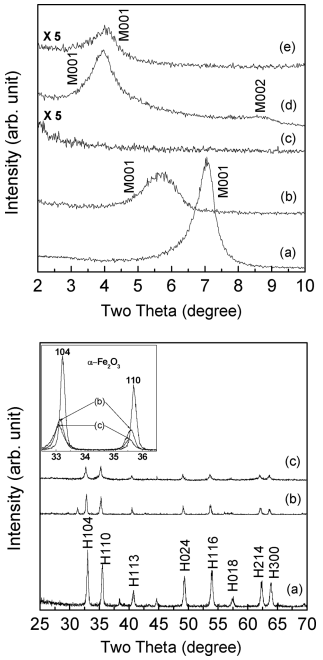

Figure 1. (Upper panel) Low-angle XRD patterns of pristine clay (montmorillonite) and hybrid particles: (a) pristine clay, (b) as-grown ICNH with 25 °C synthesized polycations, (c) 550 °C annealed ICNH with embedding 25 °C polycations, (d) as-grown particles intercalated with 70 °C synthesized polycations, and (e) 550 °C annealed ICNH with embedding 70 °C polycations, (Lower panel) XRD patterns of α-Fe_2O_3 particle and annealed hybrid particle from 25 to 70°: (a) α-Fe_2O_3 particle (with the average diameter of about 100 nm), (b) 550 °C annealed ICNH with embedding 25 °C polycations, and (c) 550 °C annealed ICNH with embedding 70 °C polycations (M denotes the reflections from montmorillonite and H denotes to the reflections from α-Fe_2O_3 (hematite)). The inset shows the change in the broadness and peak position of embedded α-Fe_2O_3 nanoparticles and reference 100 nm α-Fe_2O_3 particles.

Results and Discussion

ICNH Structure. X-ray diffraction (XRD) patterns of as-grown and thermally annealed ICNH particles that were synthesized from different polycations aged at 25 or 70 °C are presented in Figure 1. As a reference, XRD pattern of pristine clay is also added to Figure 1 (upper panel). The (00*l*) reflections of as-grown ICNH particles are found at lower 2θ than those of pristine clay particles, which provide a strong evidence for the intercalation of Fe polycations. In comparison with pristine montmorillonite having the basal distance of 0.96 nm, the lattice parameter of *c*-axis was increased to 1.47 nm for as-grown ICNH particles using 25 °C aged Fe polycations and 2.22 nm for as-grown ICNH particles using 70 °C aged Fe polycations. This result indicates that the interlayer space of ICNH particles ranges from 0.51 to 1.26 nm, depending on the intercalation method.

The thermal stability of the intercalated nanoparticles was also influenced by the nanoparticle aging method. In thermally annealed ICNH particles using 70 °C aged Fe polycations, (001) peak remained. A decrease in the intensity of (001) peak is attributed to the formation of nonuniform strain in (00*l*) planes.[16] However, in thermally annealed ICNH particles using 25 °C aged Fe polycations, the (001) peak of the montmorillonite disappeared. This suggests that ICNH particles using 70 °C aged Fe polycations have very stable Fe nanoparticles in the interlayer space. In contrast, in particles using 25 °C aged Fe polycations, thermal annealing may induce the transport of the intercalated nanoparticles onto the surface of the montmorillonite particles and weaken the long-range ordering of montmorillonite. This will be further explained in the following sections.

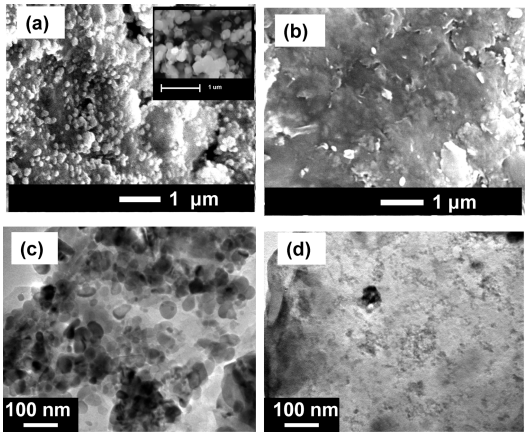

Figure 2. SEM micrographs of thermally annealed ICNH particles (a) using 25 °C synthesized polycations and (b) using 70 °C synthesized polycations. TEM micrographs of thermally annealed ICNH particles (c) using 25 °C synthesized polycations and (d) using 70 °C synthesized polycations.

As-grown ICNH particles do not show any reflections associated with α-Fe_2O_3 phase. After as-grown ICNH particles were annealed at 550 °C, additional XRD peaks assigned to 33.2, 35.7, 40.98, 62.6, and 64.2° are traced to the formation of rhombohedral hematite (α-Fe_2O_3) (Figure 1 lower panel b and c), showing the successful conversion of Fe polycations to α-Fe_2O_3 (hematite) nanoparticles.

Location of Iron Oxide in ICNH. Scanning electron microscope (SEM) images and transmission electron microscope (TEM) images of thermally annealed ICNH particles are shown in Figure 2. In hybrid particles intercalated with 25 °C grown polycations (Figure 2a), α-Fe_2O_3 particles with a size of 100 nm are observed on the surface of the montmorillonite. In contrast, the surface of hybrid particles intercalated with 70 °C grown polycations is free from 100 nm α-Fe_2O_3 particles (Figure 2b). This implies that 70 °C grown polycations are effectively intercalated into the interlayer space of montmorillonite, but a significant portion of 25 °C grown polycations are adsorbed on the surface of montmorillonite and are grown to relatively large α-Fe_2O_3 particles during subsequent thermal annealing. These SEM results are consistent with the XRD results showing larger shift in (00*l*) peaks for as-grown ICNH particles using 70 °C grown polycations. TEM images (Figure 2c, d) confirm the different location of α-Fe_2O_3 nanoparticles around montmorllionite. In the hybrid particles using 70 °C grown polycations, very small nanoparticles below 4 nm are uniformly distributed into interlayer space of montmorllionite. A very small feature of α-Fe_2O_3 nanoparticles in thermally annealed ICNH suggests that the nanoparticles are embedded between the aluminosilicate layers

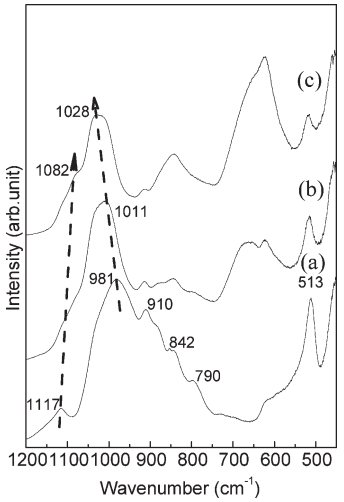

Figure 3. ATR-FTIR patterns of hybrid particles for (a) pristine clay, (b) as-grown ICNH with 25 °C synthesized polycations, and (c) as-grown ICNH with 70 °C synthesized polycations.

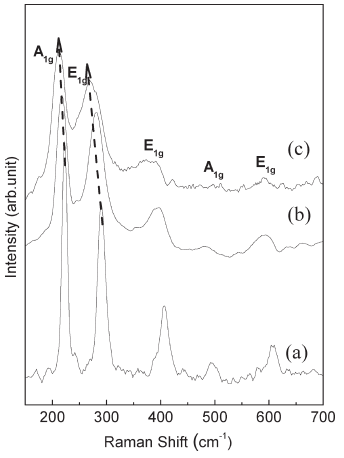

Figure 4. Raman spectra of (a) α-Fe_2O_3 particles, (b) 550 °C annealed ICNH particles using 25 °C synthesized polycations and (c) 550 °C annealed ICNH using 70 °C synthesized polycations.

and the growth of Fe polycations is prevented by the aluminosilicate layers. Therefore, in ICNH particles using 70 °C grown polycations, thermal annealing mainly crystallizes α-Fe_2O_3 nanoparticles without significantly increasing the particle size.

However, a significant portion of 25 °C grown polycations were adsorbed on the surface of montmorillonite, leading to the formation of relatively large α-Fe_2O_3 particles on the surface of clay by the thermal annealing. The structure of the hybrid particles using 25 °C grown polycations are similar to the results of the previous works showing iron oxide particles located on external surface of montmorillonite.[25] This similarity can be explained by the fact that the previous studies have also used the polycations synthesized at room temperature. However, the hybrid particles using 70 °C grown polycations results in the embedded nanoparticles that are very different from the results of the previous studies. Differences in the size and location of α-Fe_2O_3 nanoparticles can be explained by the surface charge of Fe polycation. Zeta-potential analysis of the surface charge indicates that the surface of 70 °C grown polycations (44 mV) are more positively charged than that of 25 °C grown polycations (3 mV) at pH 2 where the intercalation of polycations into the interlayer space is carried out. Therefore, 70 °C grown polycations more actively replace Na^+ cations in the interlayer space of montmorillonite than 25 °C grown polycations, which results in higher concentration of embedded hematite nanoparticles in the sample using 70 °C grown polycations.

Spectroscopic Analysis of Intercalation Behavior. The attenuated total reflection Fourier transform infrared spectroscopy (ATR-IR) spectra of pure montmorillonite and hybrid particles are shown in Figure 3. For pure montmorillonite, the bending mode of Al−Al−OH is found at 910 cm^{-1} because of the large amount of Al in the octahedral site of oxygen. The bending modes at 842 and 880 cm^{-1} represent the small amount of the impurities in pure montmorillonite, and the bending mode of Si−O−Al was observed at 513 cm^{-1}.[27] Two broad bands of as-grown ICNH particles between 600 and 900 cm^{-1} are assigned to the bending modes of Fe−O−H corresponding to α-FeOOH.[28] In Figure 3, it is noted that a shift in the peak position is clearly observed in montmorillonite intercalated with 70 °C polycations. In as-grown ICNH particles, a peak position at 981 cm^{-1} corresponding to in-plane Si−O stretching vibration of the pure montmorillonite shifts to 1011 cm^{-1} and an out-of-plane vibration mode of montmorillonite layer moves from 1117 to 1087 cm^{-1}. This systematic change in peak position of IR spectra confirms the incorporation of Fe polycations into the interlayer space of montmorillonite. When Fe polycations are intercalated, the electrostatic field between positive interlayer cations and negative Al−Si−O layers of the montmorillonite is decreased and the out-of-plane vibrations are relaxed. Therefore, the wavenumber of the out-of-plane vibrations gets decreased, whereas that of the in-plane vibrations gets increased.[29]

Figure 4 shows the Raman spectra of ICNH particles using a laser with the wavelength of 488 nm. Theoretically, α- Fe_2O_3 has seven active Raman modes ($2A_{1g} + 5E_{1g}$).[30] In Figure 4a, two A_{1g} modes are observed at 221 and 499 cm^{-1}, and four E_{1g} modes are observed at 244, 298, 410, and 620 cm^{-1} (E_{1g}). It is known that two of the E_{1g} modes between 290 and 300 cm^{-1} are a doublet and are not easily resolved. Therefore, a Raman spectrum also indicates that the thermal annealing of free Fe polycations causes the formation of α-Fe_2O_3 particles. When the Fe polycations are intercalated into the montmorillonite, Raman peaks of α-Fe_2O_3 are broadened with a shift of peak position to lower wavenumber, which is more

(27) Madejova, J.; Komadel, P. *Clays Clay Miner*. **2001**, *49*, 410.
(28) Vlasove, A. Y.; Loseva, G. V.; Sakash, G. S; Solntseva, L. S. *J. Appl. Spectrosc*. **1970**, *12*, 846.
(29) (a) Ji, Y.-Q.; Black, L.; Weidler, P. G.; Janek, M. *Langmuir* **2004**, *20*, 9796. (b) Ras, R. H. A.; Johnston, C. T.; Franses, E. I.; Ramaekers, R.; Maes, G.; Foubert, P.; De Schryver, F. C.; Schoonheydt, R. A. *Langmuir* **2003**, *19*, 4295. (c) Ras, R. H. A.; Németh, J.; Johnston, C. T.; Dékány, I.; Schoonheydt, R. A. *Thin Solid films* **2004**, *466*, 291.
(30) Bersani, D.; Lottici, P. P.; Montenero, A. *J. Raman Spectrosc*. **1999**, *30*, 355.

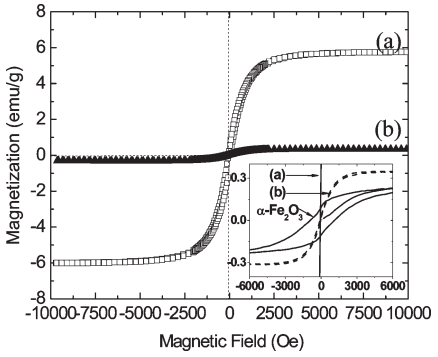

Figure 5. $M-H$ curves of thermally annealed ICNH particles using (a) 70 °C synthesized polycations and (b) 25 °C synthesized Fe polycations; an inset magnifies the $M-H$ curves of a and b and α-Fe_2O_3 particles with a size of 100 nm, near the origin.

pronounced in ICNH particles embedded with 70 °C grown Fe polycations. Because the growth of embedded α-Fe_2O_3 nanoparticles is constrained by the aluminosilicate layers, Fe−O vibrations are relaxed and corresponding Raman peaks shift to lower wavenumber. The suppression of α-phase Fe_2O_3 nanoparticles by the aluminosilicate layers also increases in the broadness of Raman peaks. Mechanical constraint by the aluminosilicate planes of the clay during the thermal annealing leaves a residual stress in the α-phase Fe_2O_3 nanoparticles, leading to increases in the broadness of Raman peaks.

Magnetic Properties. Magnetic properties of the hybrid particles were measured using vibrating sample magnetometer (VSM) at room temperature. As a reference sample, the simple mixture of clay and α-Fe_2O_3 particles was also characterized. Cation ratio of α-Fe_2O_3 nanoparticle and montmorillonite in the reference sample was controlled to be the same as ICNH particles. Before the magnetic measurement, the mixed particles were mechanically homogenized and then thermally annealed at 550 °C in N_2, which is the thermal treatment condition of ICNH particles. The results of VSM measurements are shown in Figure 5. The $M-H$ curve of the α-Fe_2O_3 nanoparticle−montmorillonite mixture exhibits a hysteresis loop. Its remanent magnetization and coercivity are 0.05 emu/g and 500 Oe, respectively. Given that α-Fe_2O_3 with a canted ferromagnetism due to deflection of the magnetic dipoles from the antiferromagnetic plane has a saturated magnetization (M_s) of 0.22 emu/g and a coercive field of 600 Oe, the magnetic properties of the mixture can be explained using a mixture rule. When the magnetic properties of α-Fe_2O_3 and montromorillonite are averaged on the basis of their ratio, the calculated results are very similar to the experimental observations in Figure 4. The $M-H$ curve of the hybrid particles, however, is very different from that of α-Fe_2O_3. First, the saturated magnetization of the hybrid particles is much larger than that of the mixture and the increase in the magnetization is more significant in the hybrid particles using 70 °C Fe polycations. The saturated magnetization is 0.34 emu/g for ICNH particles using 25 °C Fe polycations and 5.98 emu/g for ICNH particles using 70 °C Fe polycations. The saturated magnetization per Fe ion of ICNH particles is at most about 60 times larger than that of 100 nm α-Fe_2O_3 nanoparticles. Second, ICNH particles exhibit negligible coercive field, regardless of their very large saturated magnetization. A combination of huge saturated magnetization and nearly zero coercive field of ICNH particles cannot be traced to the magnetic properties of α-Fe_2O_3 showing a small saturated magnetization and a large coercive field. Instead, the differences in the location and size of α-Fe_2O_3 nanoparticles in Figures 1−4 provide a way to explain the superior superparamagnetic properties of ICNH particles.

Origin of Magnetic Anisotropy. The introduction of α-Fe_2O_3 nanoparticles into the interlayer space of the montmorillonite are expected to cause three following effects. First, because the aluminosilicate layers prevent the embedded α-Fe_2O_3 nanoparticles from growing, only the crystallization and densification of the embedded α-Fe_2O_3 nanoparticles are allowed during thermal annealing. As a result, the size of α-Fe_2O_3 nanoparticles remains at several nanometers, though their crystallinity is as high as that of large particles. This suppressed growth of embedded α-Fe_2O_3 nanoparticles is responsible for the disappearance of the hysteresis in the $M-H$ curve of ICNH particles. As the size of ferromagnetic materials decreases to about a few nanometers, thermal fluctuation dominates the ordering of magnetic dipoles. Therefore, the coercivity and remanent magnetization become nearly zero under zero magnetic field, which is called as superparmagnetism.[6] Second, the suppressed growth of the embedded α-Fe_2O_3 nanoparticles by the aluminosilicate layers builds up internal stress in the α-Fe_2O_3 nanoparticles, as shown in XRD patterns and Raman spectra (Figure 1 inset and Figure 4). Because the mechanical constraint is provided by two-dimensional aluminosilicate layers, α-Fe_2O_3 nanoparticles are exposed to uniaxial compressive stress normal to the aluminosilicate layers. In other words, two-dimensional tensile strain parallel to aluminosilicate layers is developed in the embedded nanoparticles. Third, the mechanical stress in the hybrid particles develops unique magnetic response. It is well-known that the application of anisotropic stress to ferromagnetic materials can significantly affect the alignment of the magnetic dipoles along a specific direction and modify the magnetization.[31] The magnetic anisotropy is determined by the sum of magnetocrystalline anisotropy energy and magnetoelastic energy. As a significant amount of uniaxial stress is applied to produce biaxial strain, the change in the magnetoelastic becomes dominant over the mangetoanistropy energy. The distribution of the strain is then closely related to the easy direction of the magnetization. This indicates that the

(31) (a) Cullity, B. D. *Introduction to Magnetism and Magnetic Materials*; Addison-Wesley: Reading, MA, 1972. (b) Wang, J.; Neaton, J. B.; Zheng, H.; Nagarajan, V.; Ogale, S. B.; Liu, B.; Viehland, D.; Vaithyanathan, V.; Schlom, D. G.; Waghmare, U. V.; Spaldin, N. A.; Rabe, K. M.; Wuttig, M.; Ramesh, R. *Science* **2003**, *299*, 1719. (c) Zheng, H.; Wang, J.; Lofland, S. E.; Ma, Z.; Mohaddes-Ardabili, L.; Zhao, T.; Salamanca-Riba, L.; Shinde, S. R.; Ogale, S. B.; Bai, F.; Viehland, D.; Jia, Y.; Schlom, D. G.; Wuttig, M.; Roytburd, A.; Ramesh, R. *Science* **2004**, *303*, 661.

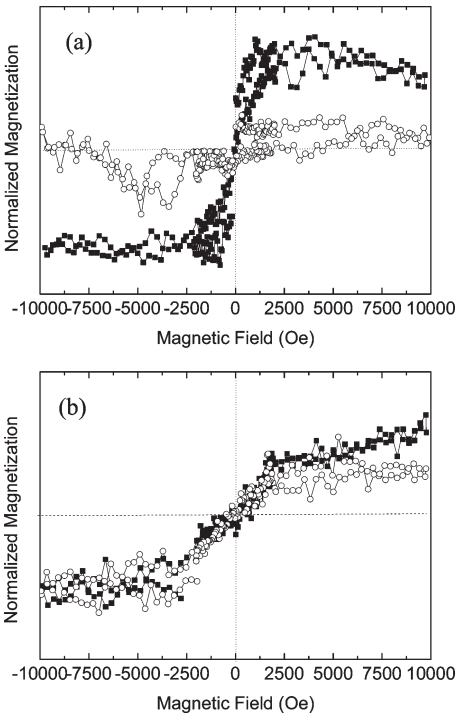

Figure 6. Normalized $M-H$ curves of (a) annealed ICNH on glass substrate and (b) α-Fe_2O_3 particles on glass; in-plane magnetization (solid square) and out-of-plane magnetization (open circle).

unique antiparallel arrangement of the magnetic dipoles responsible for the canted ferromagnetism of α-Fe_2O_3 nanoparticles may not be valid for α-Fe_2O_3 nanoparticles that are exposed to the anisotropic stress. According to intensive studies on the correlation between stress and ferromagnetism (or ferrimagnetism), the magnetic dipoles are realigned to be parallel to tensile strain and the saturated magnetization along the direction of the tensile strain can be significantly enhanced.[32]

During subsequent thermal annealing, the aluminosilicate layers suppress the growth of α-Fe_2O_3 nanoparticles and apply a uniaxial stress to α-Fe_2O_3 nanoparticles. It could be found that magnetic interaction between α-Fe_2O_3 nanoparticles under uniaxial stress dramatically increases the saturated magnetization of the hybrid particles with maintaining zero remanence magnetization. Hence, their magnetic anisotropy was characterized to find an origin for the large magnetization of ICNH particles. ICNH particles were dispersed in water and deposited on the glass by a spin-coating method. The magnetic field was then applied to be parallel to or normal to the surface of ICNH particle films for the magnetic measurements. Because the hybrid particles have highly anisotropic two-dimensional shape, the aluminosilicate layers were placed to be parallel to the surface of the glass

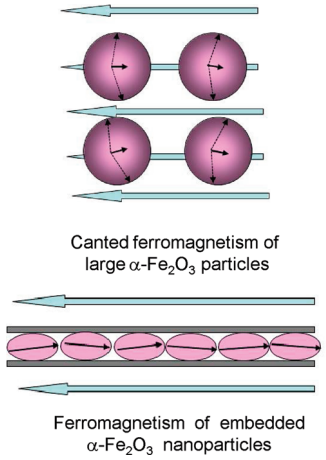

Figure 7. Schematics explaining the very small size, elongated shape, uniaxial stress, and enhanced magnetization of the hybrid particles (canted ferromagnetism of bulk α-Fe_2O_3 particles is also shown as a reference).

plates during a spin coating. Therefore, a change in the direction of the magnetic field enabled us to quantitatively measure in-plane and out-of-plane magnetization of two-dimensional ICNH particles. As a reference sample, pure α-Fe_2O_3 particle films were prepared by spin-coating 100 nm α-Fe_2O_3 particles on the glass. $M-H$ curves of ICNH particle films and α-Fe_2O_3 particle films under the magnetic field parallel or perpendicular to the surface of the films are shown in Figures 6. Solid squares present the magnetic response of the hybrid particle films to parallel magnetic field. The magnetization of ICNH particle films changes dramatically as the parallel magnetic field sweeps from -2500 to 2500 Oe. The shape of $M-H$ curve under the parallel magnetic field is very similar to that of the randomly oriented hybrid particles. When the magnetic field was perpendicular to the main surface of the hybrid particle films, the magnetization gets much smaller and its dependence on the magnetic field becomes negligible (open circle in Figure 6a). However, in α-Fe_2O_3 particle films, in-plane and out-of-plane magnetizations are very similar (Figure 6b). Magnetic anisotropy observed only in ICNH particle films indicates that a hybridization of montmorillonite matrix and embedded α-Fe_2O_3 nanoparticles has developed a peculiar magnetic anisotropy, leading to the dramatic increase in their saturated magnetization. The aforementioned effects of the aluminosilicate layers on the structure and magnetization of hybrid particles are schematically presented in Figure 7.

Magnetorheological Properties. As a proof of concept experiment for the use of new ICNH nanoparticles, we prepared aqueous fluids containing new ICNH particles. Due to their unique physical properties like strong thixotropic and gelation behavior, montmorillonite based fluids are being widely used in various applications.[33] In addition to a fluid containing 5 wt % thermally annealed

(32) (a) Chen, Y. Z.; Sun, J. R.; Han, Y. N.; Xie, X. Y.; Shen, J; Rong, C. B.; He, S. L.; Shen, B. G. *J. Appl. Phys.* **2008**, *103*, 07D703. (b) Brandlmaier, A.; Geprägs, S.; Weiler, M.; Boger, A.; Opel, M.; Huebl., H; Bihler, C.; Brandt, M. S.; Botters, B.; Grundler, D.; Gross, R.; Goennenwein, S. T. B. *Phys. Rev. B* **2008**, *77*, 104445. (c) Chambers, S. A.; Farrow, R. F. C.; Maat, S.; Toney, M. F.; Folk, L.; Catalano, J. G.; Trainor, T. P.; Brown, G. E. *J. Magn. Magn. Mater.* **2002**, *246*, 124. (d) Park, S; Zhang, X; Misra, A.; Thompson, J. D.; Fitzsimmons, M. R.; Lee, S.; Falco, C. M. *Appl. Phys. Lett.* **2005**, *86*, 042504.

(33) (a) Darley, H. C. H.; Gray G. R. In *Composition and Properties of Drilling and Completion Fluids*, 5th ed.; Gulf Publishing: Houston, TX, 1988.; (b) Dolz, M.; Jiménez, J.; Jesús Hernández, M.; Delegido, J.; Casanovas, A. *J. Pet. Sci. Eng.* **2007**, *57*, 294.

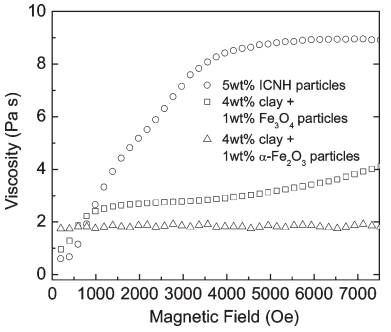

Figure 8. Viscosity vs magnetic field of aqueous fluid containing 5 wt % thermally annealed ICNH particles using 70 °C synthesized polycations (open circle), the mixture of 1 wt % Fe_3O_4 particles and 4 wt % montmorillonite particles (open square)l and the mixture of 1 wt % α-Fe_2O_3 particles and 4 wt % montmorillonite particles (open triangle).

ICNH particles using 70 °C synthesized polycations, two reference samples are prepared. One is the mixture of 1 wt % α-Fe_2O_3 particles and 4 wt % montmorillonite, and the other is the mixture of 1 wt % Fe_3O_4 nanoparticles and 4 wt % montmorillonite. Fe_3O_4 nanoparticles were selected, because their magnetization per Fe ion is close to that of ICNH particles. Figure 8 shows the effect of magnetic field on the viscosity of the fluids. The viscosity of an aqueous fluid containing 5 wt % hybrid particles increased almost 16 times when the applied magnetic field reached 3500 Oe, which is consistent with $M-H$ curve in Figure 5. In contrast, the mixture of clay and α-Fe_2O_3 particles did not show a meaningful increase in the viscosity under the magnetic field. A big increase in the viscosity of the ICNH particles under the magnetic field is attributed to the rotation of the hybrid particles as well as their higher magnetization. Figure 9 schematically shows the difference between the ICNH particles and the simple mixture. When magnetic field is not applied, the hybrid particles are aligned in parallel to flow direction of fluid. However, magnetic field normal to stream direction of fluid align the magnetically easy axis of hybrid particles parallel to the magnetic field direction. When the layers of hybrid particles in fluid are rotated to be perpendicular to the flow direction, the internal friction of fluid flow increases because of the magnetically aligned ICNH particles. On the other hand, for the fluids containing iron oxide/clay mixture, only magnetically active Fe_3O_4 or α-Fe_2O_3 particles are realigned by the external magnetic field. Paramagnetic clay with weak saturated magnetization do not respond to the magnetic field.[34]

(34) Levin, E. M.; Hou, S. −S.; Budko, S.; Schmidt-Rohr, K. *J. Appl. Phys.* **2004**, *96*, 5087.

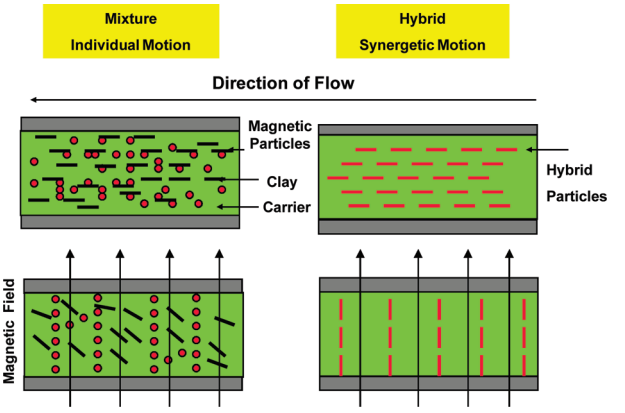

Figure 9. Schematic illustration of particle motion in the fluids with and without the magnetic field whose direction is perpendicular to the fluid moving direction.

Therefore, the ICNH particle using 70 °C synthesized polycations provides much larger magnetic field dependence to the fluids than the simple mixture.

Conclusion

In summary, new iron oxide−clay hybrid particles were synthesized through the ion exchange method. The size and location of α-Fe_2O_3 nanoparticles depend on the surface properties of Fe polycations. When Fe polycations were aged at 70 °C, Fe polycations are easily introduced to the interlayer space and are converted to α-Fe_2O_3 nanoparticles during subsequent thermal annealing. α-Fe_2O_3 nanoparticles embedded in the interlayer space shows about 60 times increase in the saturated magnetization per Fe atom with nearly zero coercive field. This unique combination of the magnetization and the coercivity is traced to the suppressed growth of embedded α-Fe_2O_3 nanoparticles by the aluminosilicate layers, leading to the size control, anisotropic magnetic interaction, and uniaxial stress of two-dimensionally distributed α-Fe_2O_3 nanoparticles. Moreover, new ICNH particles provide a new functionality to the aqueous fluids. When new ICNH particles are added to the aqueous fluids, the viscosity of the fluids shows a big change under the magnetic field. This is attributed to the fact that the embedded α-Fe_2O_3 nanoparticles allows for the rotation of ICNH particles by the external magnetic field.

Acknowledgment. This work was supported by the U.S. Department of Energy. The authors thank Dr. Ian Nettleship and Dr. Prashant Kumta for very helpful technical discussions.